Supplemental information

Direct Observation of the Myosin Va Recovery Stroke That Contributes to Unidirectional Stepping along Actin

Katsuyuki Shiroguchi[1¤]*, Harvey F. Chin[2], Diane E. Hannemann[2], Eiro Muneyuki[3], Enrique M. De La Cruz[2]*, Kazuhiko Kinosita Jr.[1]

[1] Department of Physics, Faculty of Science and Engineering, Waseda University, Tokyo, Japan, [2] Department of Molecular Biophysics and Biochemistry, Yale University, New Haven, Connecticut, United States of America, [3] Department of Physics, Faculty of Science and Technology, Chuo University, Tokyo, Japan

* E-mail: kshirog@fas.harvard.edu (KS); enrique.delacruz@yale.edu (EMD)
¤ Current address: Department of Chemistry and Chemical Biology, Harvard University, Cambridge, Massachusetts, United States of America

PLoS Biol 2001, 9(4): e1001031.

Figures S1-8
(References in the figure captions of S1-8 are in the main text)

Caption of Video S1

Protocol S1

References for Protocol S1

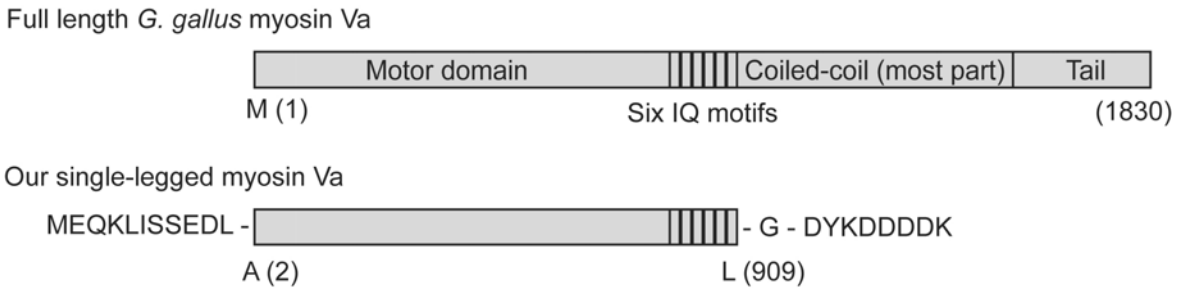

Figure S1 Myosin Va construct used in this study.
Amino acid residues are shown by single letters. Sequence numbers in parentheses refer to the original full-length construct. Note that the second amino acid (Ala) in chicken myosin Va is seen in a crystal structure [15], suggesting that the N-terminus takes a stable conformation. Moreover, though only pre-recovery stroke conformation has been solved by high resolution for myosin Va [15], for myosin II, the N-terminal domain consists of a head (motor domain) that takes distinct angle (~70°) relative to the neck portion (lever arm) in pre-recovery stroke and post-recovery stroke conformations [15].

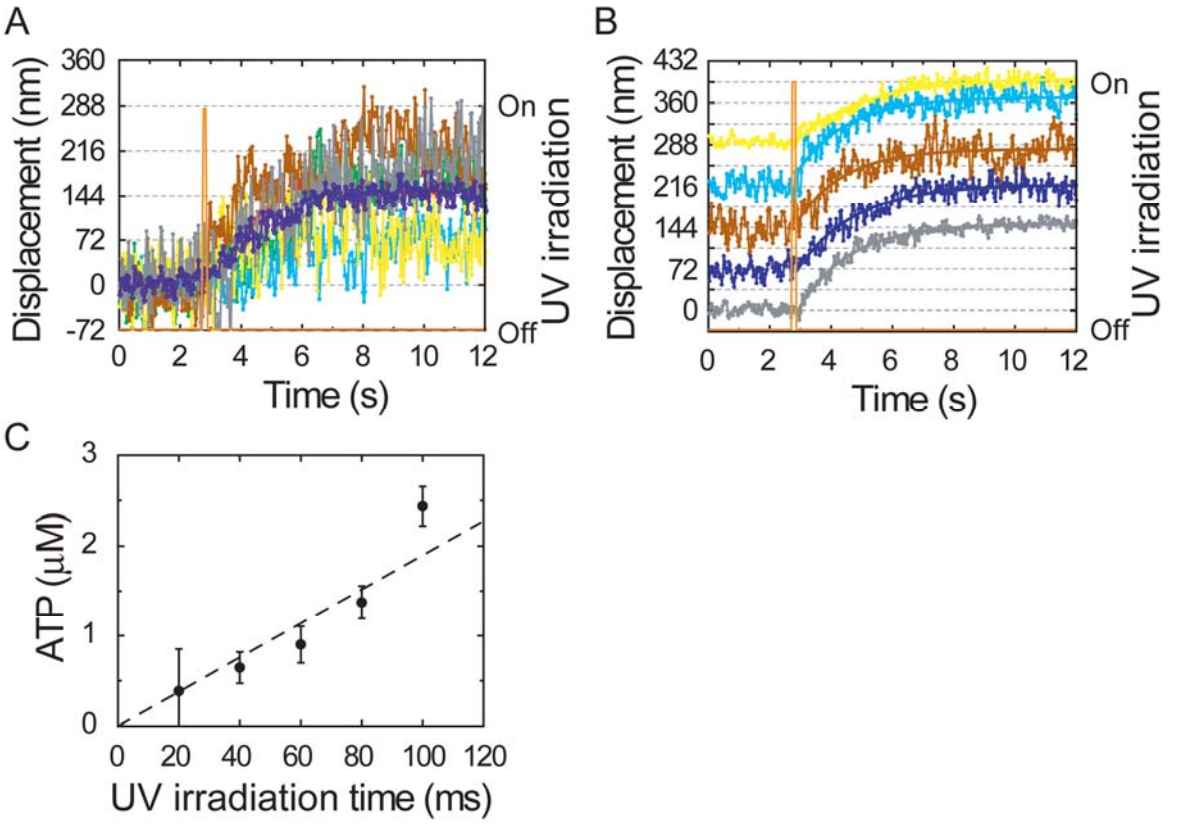

Figure S2 Estimation of UV-generated ATP concentration and its decay time by the gliding bead assay. (A)Time courses of the gliding of a myosin-coated bead on actin after a 100% UV flash for 0.1 s (indicated in orange). Those beads that moved straight (because the actin filament was straight on a surface) were selected for the analysis. Different colors show different beads, dark blue being the average of all records. (B) Displacement records averaged over five or more moving beads, as in (A) (dark blue), in five different chambers distinguished by color. The UV intensity was 100% and duration, 0.1 s. The time courses were fitted with an exponential (smooth lines), giving an average time constant of 1.8±0.3 s (s.d. for the five records shown) for the decay of [ATP] by apyrase. (C) The initial ATP concentration generated by a single UV flash of varying duration at 100% UV intensity. The initial gliding velocity estimated from the exponential fit as in (B) was converted to [ATP] by assuming that the native myosin Va carrying the bead made 36-nm steps by binding ATP at the rate constant of 0.9×10^6 $M^{-1}s^{-1}$ [23]. A linear fit (broken line) indicates that, at 100% UV intensity, ATP is generated at a rate of ~20 μM s^{-1}. A separate set of experiments (not shown) indicated that this rate is proportional to the UV intensity between 0.7%–100%. Bars, standard error.

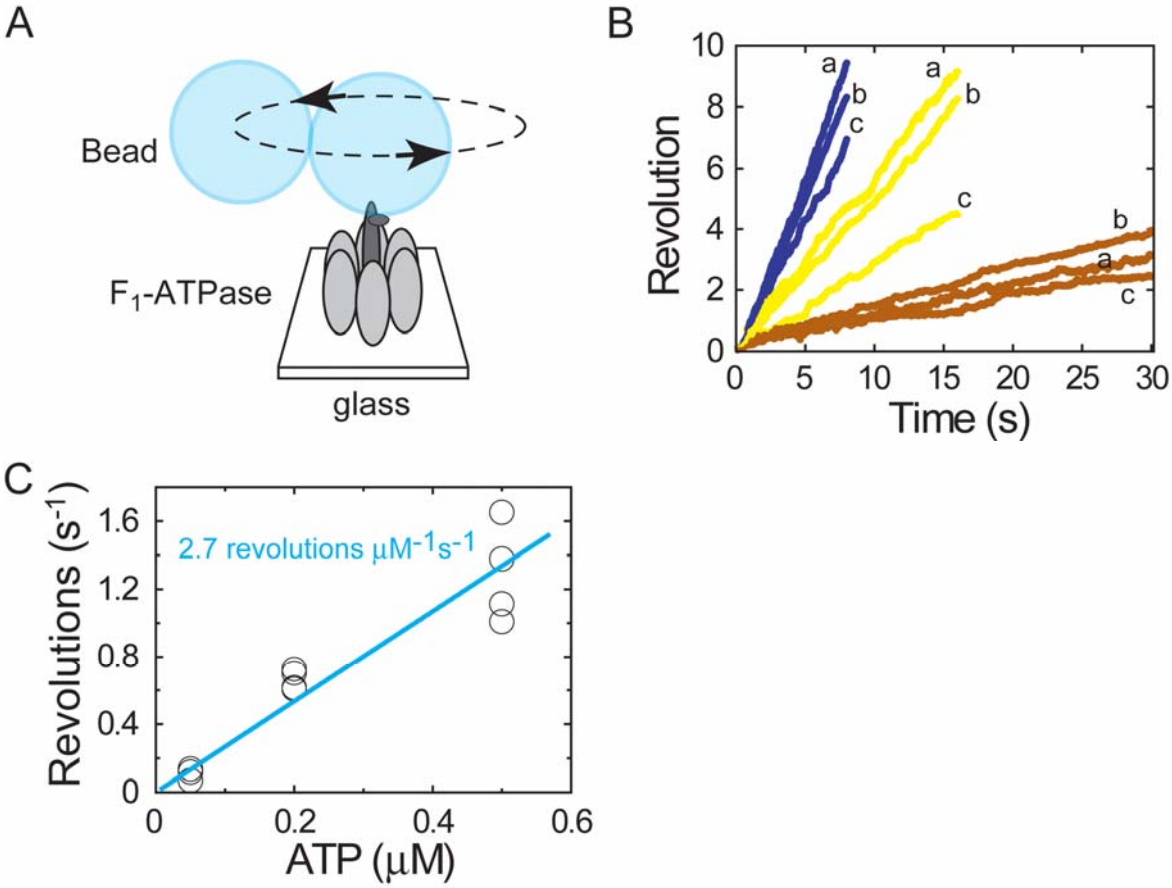

Figure S3 Generation of quasi-stationary [ATP] confirmed by the rotary motor F_1-ATPase (GT mutant). (A) Observation system (not to scale). The stator (gray; $\alpha_3\beta_3$ subunit) is adsorbed on a glass surface, and a duplex of streptavidin-coated beads is attached to the biotinylated rotor (black; γ subunit). (B) Rotation of three molecules (a–c) under different UV intensities (color-coded as in Figure 2B). Each molecule was subjected to different intensities repeatedly as in Figure 2B, which is a partial record for molecule b, and each curve in (B) represents an average of >6 rotation time courses obtained under the same intensity. (C) ATP dependence of the rotational speed with regular ATP. Bead duplexes that rotated relatively fast and smoothly were selected, and the average speed over >20 contiguous revolutions (ten for one molecule at 0.05 μM ATP) was determined. The apparent rate constant of ATP binding, based on the assumed consumption of three ATP molecules per turn, is 8.1 (= 2.7 × 3) $\mu M^{-1}s^{-1}$, comparable with the values previously reported for this mutant (1.8 $\mu M^{-1}s^{-1}$ in a rotation assay, 4.2 or 6.8 $\mu M^{-1}s^{-1}$ for bulk ATPase activity) [21,22].

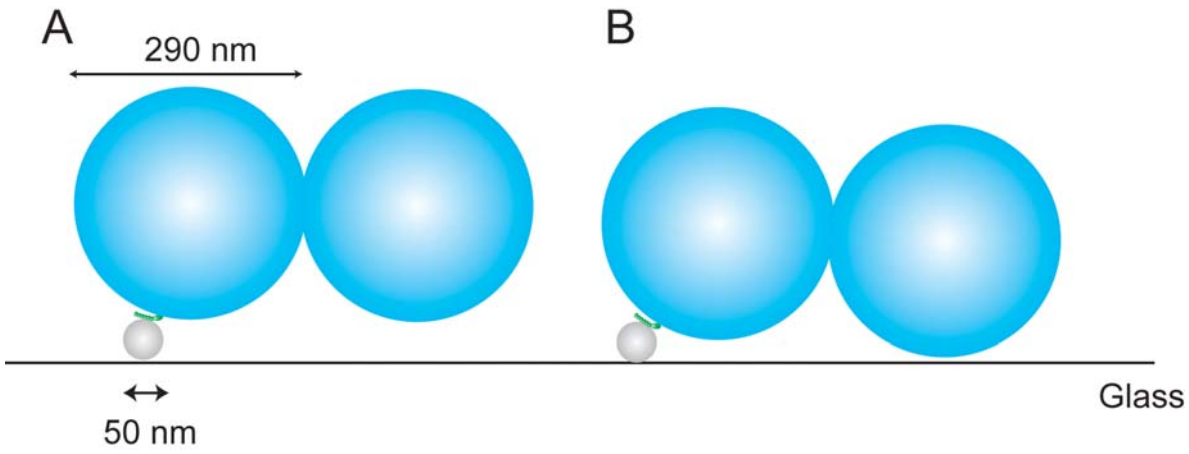

Figure S4 Configuration of myosin and beads drawn to scale.
Examples of configurations in which large duplex beads can swing (A) and cannot swing (B). Myosin (in green) is between two sizes of beads: other proteins shown in Figure 1B are not shown here. The myosin neck is immobilized on a small gray bead, and the head is attached to a large blue duplex. Myosin binding to small and large beads occurs by chance. Duplex bead swinging occurs only when conditions under which the swinging beads do not collide with the surface are satisfied: (i) myosin is on the top of the small bead, (ii) myosin is properly oriented such that the swing plane is parallel to the surface, and (iii) the long axis of duplex beads is almost parallel to a surface. These conditions contribute to a low frequency of observed bead swinging.

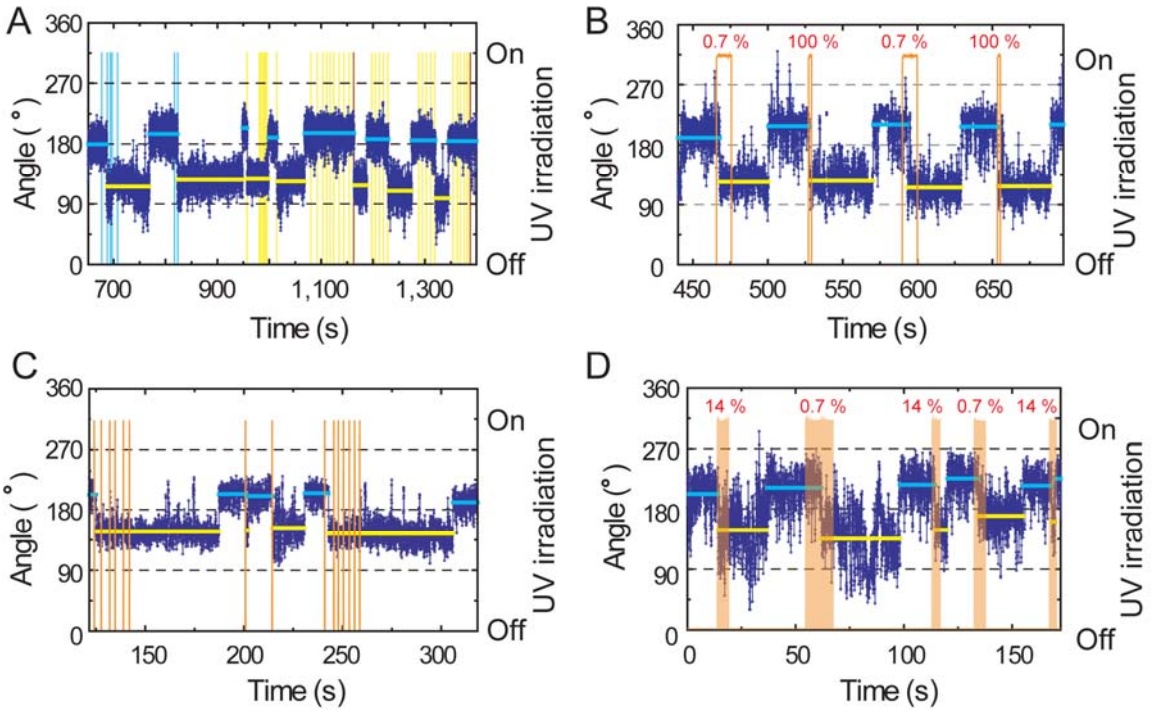

Figure S5 Head–neck swings of myosin Va under different UV irradiation conditions. Dark blue dots with a light gray line indicate angular positions of the beads on the head at 33-ms intervals (video frame rate); horizontal cyan lines indicate average angles before UV irradiation (pre-recovery stroke state); yellow lines indicate average angles after irradiation (post-recovery stroke state). (A) Single UV flashes of different powers. Vertical cyan lines indicate 100% intensity for 10 ms; yellow indicates 25% for 10 ms; brown indicates 25% for 100 ms. Compared to Figure 1C, where a 100-ms flash at 100% intensity always induced a return swing, short (10 ms) and/or weak (25%) flashes here often had to be applied several times before a successful return swing was observed, indicating that the swings depend on UV-generated ATP. (B) Continuous UV irradiation at 100% and 0.7% intensities for 2 s and 10 s, respectively. Under 100% UV, a swing was observed at 0.74 s on average (seven swings in three molecules), and under 0.7%, at 3.2 s (eight swings). Under continuous irradiation, [ATP] would rise toward the steady-state value of 50 μM at 100% (the generation rate of 20 μM divided by the depletion rate of 1/[2–3 s]) or 0.4 μM at 0.7%, with the time constant of 2–3 s (Figures S2 and S3). The observed waiting times above are thus consistent with ATP binding to myosin Va with the bimolecular rate constant of 1.7×10^6 $M^{-1}s^{-1}$ measured in the stopped flow apparatus (Protocol S1). (C) UV flashes (100%, 0.2 s) in the post-recovery stroke state. None induced a swing back to the pre-recovery stroke state. (D) Quasi-steady ATP levels generated by the patterned irradiation in Figure 2A at indicated intensities. This is another example of the experiment in Figure 3A.

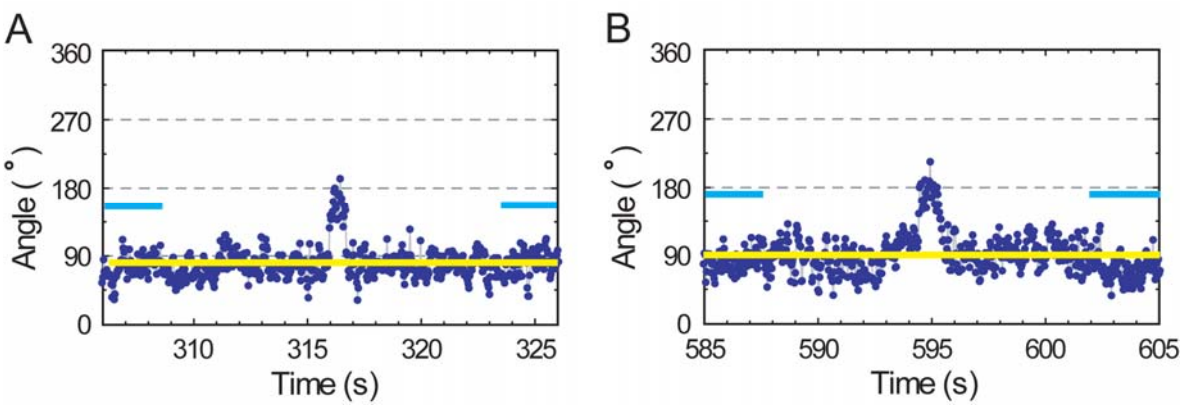

Figure S6 Momentary reversals to the pre-recovery stroke angle during post-recovery stroke states.
(A and B) Dark blue dots with a light gray line indicate the angular positions of the beads on the head at 33-ms intervals (video frame rate); yellow indicates the average angle of the post-recovery stroke state; cyan indicates the pre-recovery stroke state before (left) and after (right) the shown post-recovery stroke state. These are expanded parts of the time course in Figure 1C, around two arrow heads.

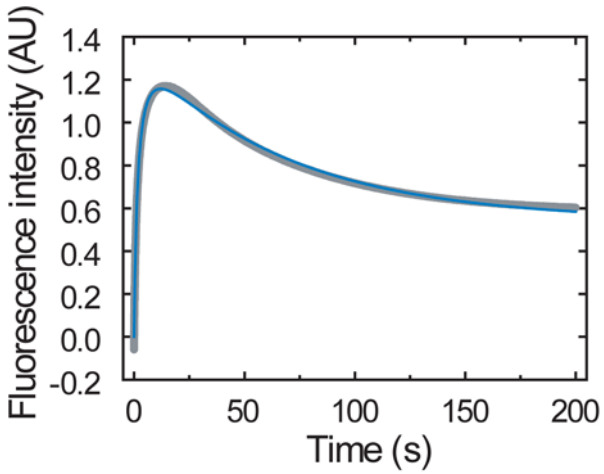

Figure S7 Time course of fluorescence change after mixing 1.0 µM monomeric myosin Va with 0.4 mM MgmantATP. The increase in fluorescence represents mantATP binding. The reduction results from mantADP release, which is limited by P*i* release [23]. The data (gray) represent an individual, unaveraged time course of fluorescence change after subtraction of a baseline from mantATP photobleaching. The smooth line (cyan) through the data represents the best fit and yields a mantATP association rate constant of 1.57 (± 0.002) μM^{-1} s^{-1} and a P*i* release rate constant of 0.019 (± 0.001) s^{-1}. A P*i* release rate constant measured with ATP was 0.028 (± 0.001) s^{-1}. These are consistent with our previous measurements for a shorter neck construct (P*i* release, 0.02 s^{-1}) [23].

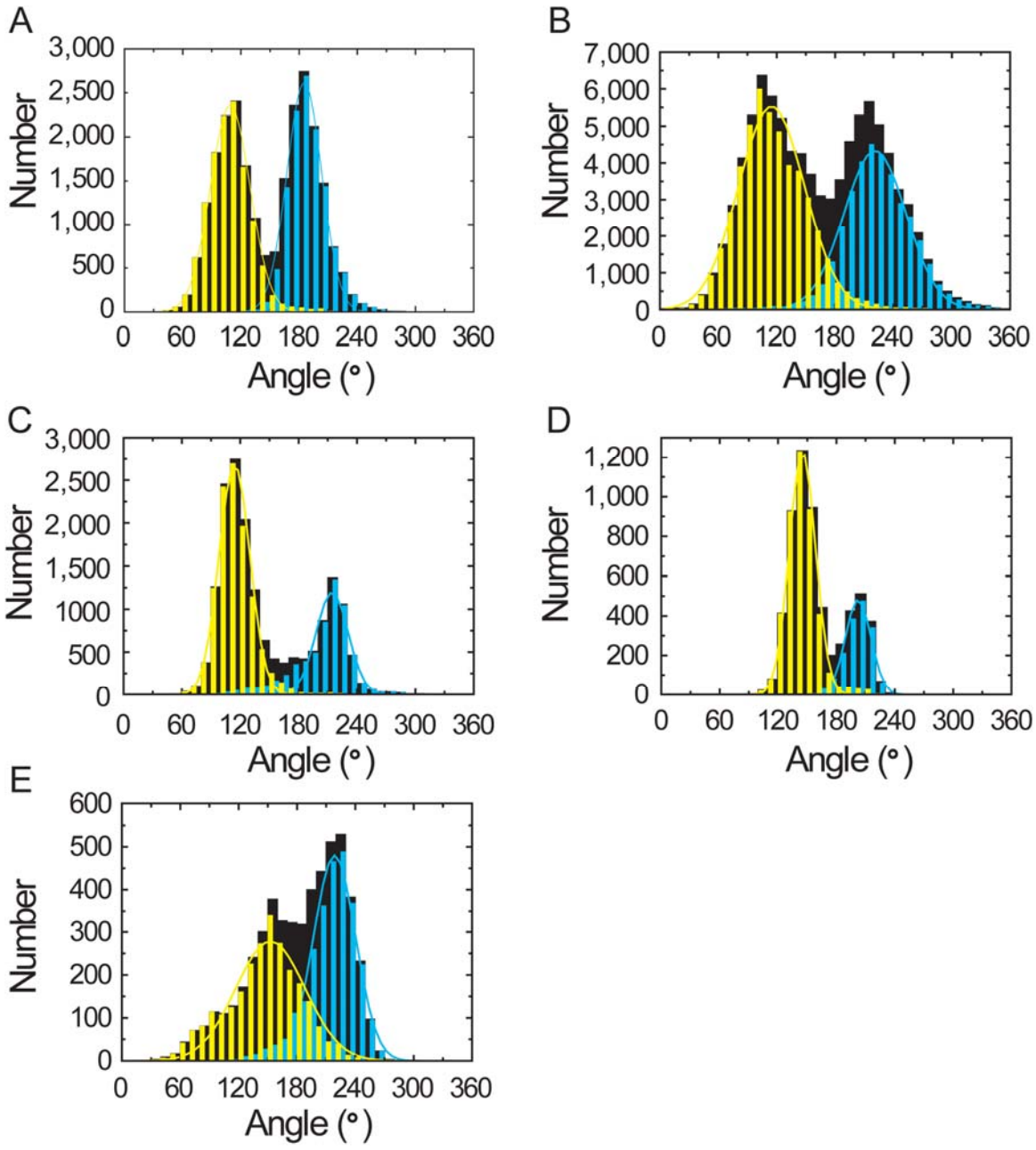

Figure S8 Distributions of bead angles in the prerecovery stroke (cyan) and post-recovery stroke (yellow) states.
Black bars indicate whole frames. These are additional examples of the analysis in Figure 5A. (A–E) Distributions for Figures 1C, 3A, and S5B–S5D, respectively. Lines show Gaussian fits: $\exp[-(\theta - \theta_m)^2/2\sigma^2]$where θ_m is the mean angle.

Video S1 Motion of an aggregate of beads (0.29 μm in diameter) attached to the head of monomeric myosin Va. Contrast and brightness have been modified (30 frames s^{-1}). White bars that appear in the left panel indicate UV irradiations. The video presents approximately the interval 260 s to 370 s in the time course of Figure 1C.

Protocol S1

Materials. Native myosin V was purified from chick brain as previously reported (1). Rabbit skeletal actin was prepared (2), biotinylated (biotin-$(AC_5)_2$-Sulfo-Osu, Dojindo Laboratories), and stained with Alexa Fluor 488 phalloidin (ref. 3) (Invitrogen). Biotinylated α-casein was made by mixing unphosphorylated α-casein (Sigma) with biotin-$(AC_5)_2$-Sulfo-Osu and was purified by gel chromatography. A GT mutant (4, 5) of the rotary motor F_1-ATPase was expressed in *E. coli* and its rotor (the γ subunit) was biotinylated at the two genetically introduced cysteines.

Gliding bead assay. The gliding velocity of myosin-coated beads on surface-immobilized actin filaments was examined to estimate the concentration of ATP generated by UV irradiation. All solutions below were in buffer A and the following infusions (2-3 chamber volumes) were made with 1-2 min incubation times in between: 0.13 mg mL^{-1} biotinylated unphosphorylated α-casein, 2 mg mL^{-1} unbiotinylated, unphosphorylated α-casein, 1 mg mL^{-1} streptavidin, buffer A for washing, 200 nM biotinylated alexa 488 labeled actin, buffer A for washing. Finally, native myosin V-bead complex (myosin V mixed with 0.34 μm carboxylated polystyrene beads (Polysciences) at the molar ratio of 5:1 and incubated for more than 2 min) was infused together with 200 μM caged ATP, 1.7 mU μL^{-1} apyrase, 1 mg mL^{-1} unphosphorylated α-casein, an oxygen scavenger system (3.2 mg mL^{-1} glucose, 0.2 mg mL^{-1} glucose oxidase, and 0.89 mg mL^{-1} catalase), and 0.5 % (v/v) β-mercaptoethanol. UV irradiation was initiated after the myosin-coated beads had settled on the surface-immobilized actin filaments.

F_1–ATPase rotation assay. The GT mutant of F_1-ATPase which, unlike the wild type, does not readily adopt an inhibited state (4, 5) was adsorbed on a clean glass surface and the rotation of a streptavidin-coated bead duplex attached to the biotinylated rotor (γ subunit) was observed (Figure S3A) (ref. 6). All solutions below were in buffer A and the following infusions (2-3 chamber volumes) were made with 1-2 min incubation in between: 4 -20 nM GT mutant, 5 mg mL^{-1} BSA, 0.29-μm streptavidin coated beads (Seradyn, washed three times by centrifugation with buffer A) together with 200 μM ATP (Sigma) and 3.8 mg mL^{-1} BSA, buffer A for washing. Finally, 200 μM caged ATP and 1.7 mU μL^{-1} apyrase. Rotating beads were identified upon UV excitation. After allowing apyrase to deplete generated ATP, we monitored rotation under several UV irradiation conditions (Figures 2, S3). In the case of ATP-dependent rotation, bead solution did ont contain ATP, and the final infusion solution contained ATP (0.05 – 0.5 μM) and an

ATP-regenerating system (1 mM creatine phosphate and 0.1 mg mL^{-1} creatine kinase) instead of caged ATP and apyrase.

Transient kinetic analysis. Transient kinetic fluorescence measurements were performed with single-headed myosin Va (7) using an Applied Photophysics SX.18MV-R stopped flow apparatus thermostatted at 25±0.1 ºC. All experiments were performed in KMg50 buffer (50 mM KCl, 2 mM $MgCl_2$, 1 mM EGTA, 1 mM DTT, and 10 mM imidazole, pH 7.0). A molar equivalent of $MgCl_2$ was added to ATP and mant-ATP immediately before use. Uncertainties are reported as standard errors in the fits. Concentrations stated are final after mixing.

Mant-ATP binding kinetics were measured by Förster resonance energy transfer from myosin V tryptophan residues (λ_{ex}=280 nm) to bound fluorescent mant-nucleotide under pseudo-first-order conditions with [nucleotide] >> [myosin V] (ref 7, 8). Fluorescence was monitored at 90° through a 400-nm, long-pass colored glass filter. The assay was performed twice or more in each ATP concentration (5, 10, 15, 20, 25, 35, 50 and 125 μM). Time courses of nucleotide binding were fit to single exponentials using software provided with the instrument. The ATP association rate constant of 1.7 (± 0.1) $\times 10^6$ $M^{-1}s^{-1}$ was determined from the best linear fit of the concentration-dependence of the observed reaction rate constants (9).

Single turnover experiments were performed by mixing 0.4 μM ATP or mant-ATP (λ_{ex} = 280 nm) with excess (1 μM) monomeric myosin V. Fluorescence was monitored at 90° through a Schott 320WG filter or a 400-nm, long-pass colored glass filter for ATP or mant-ATP binding, respectively. Time courses were fit by numerical simulation using KinTek Global Kinetic Explorer following a three-step model with initial ATP binding under non-pseudo-first order conditions followed by slow, rate-limiting P_i release then rapid ADP release (7). The ATP hydrolysis rate constant is rapid (7) and does not contribute to the observed relaxations.

References for Protocol S1

1. Cheney RE (1998) Purification and assay of myosin V. *Methods Enzymol.* **298:** 3-18.

2. Spudich JA, Watt S (1971) The regulation of rabbit skeletal muscle contraction. I. Biochemical studies of the interaction of the tropomyosin-troponin complex with actin and the proteolytic fragments of myosin. *J. Biol. Chem.* **246:** 4866-4871.

3. Ali MY, *et al.* (2002) Myosin V is a left-handed spiral motor on the right-handed actin helix. *Nat. Struct. Biol.* **9:** 464-467.

4. Nishizaka T, *et al.* (2004) Chemomechanical coupling in F_1-ATPase revealed by simultaneous observation of nucleotide kinetics and rotation. *Nat. Struct. Mol. Biol.* **11:** 142-148.

5. Muneyuki E, *et al.* (2007) Single molecule energetics of F_1-ATPase motor. *Biophys. J.* **92:** 1806-1812.

6. Yasuda R, Noji H, Yoshida M, Kinosita K Jr, Itoh H (2001) Resolution of distinct rotational substeps by submillisecond kinetic analysis of F_1-ATPase. *Nature* **410:** 898-904.

7. De La Cruz EM, Wells AL, Rosenfeld SS, Ostap EM, Sweeney HL (1999) The kinetic mechanism of myosin V. *Proc. Natl. Acad. Sci. USA* **96:** 13726-13731.

8. Henn A, De La Cruz EM (2005) Vertebrate myosin VIIb is a high duty ratio motor adapted for generating and maintaining tension. *J. Biol. Chem.* **280:** 39665-39676.

9. De La Cruz EM, Ostap EM. (2009) Kinetic and equilibrium analysis of the myosin ATPase. *Methods Enzymol*. **455** 157-92.